Carrier-envelope-phase–controlled molecular dissociation by ultrashort chirped laser pulses

S. A. Bozpolat,[1] P. Rosenberger,[2,3] M. F. Ciappina,[2,4] M. F. Kling,[2,3] and I. Yavuz[1]

[1]*Physics Department, Marmara University, 34722 Ziverbey, Istanbul, Turkey*

[2]*Max-Planck-Institut für Quantenoptik, Hans-Kopfermann-Straße 1, D-85748 Garching, Germany*

[3]*Department of Physics, Ludwig-Maximilians-Universität Munich, Am Coulombwall 1, D-85748 Garching, Germany*

[4]*Institute of Physics of the ASCR, ELI-Beamlines, Na Slovance 2, 182 21 Prague, Czech Republic*

(Received 3 July 2019; revised manuscript received 7 October 2019; published 5 December 2019)

We demonstrate and characterize that a carrier-envelope-offset-phase (CEP)–controlled ultrashort chirped field is an efficient and robust mechanism to modify the dissociation dynamics of molecular hydrogen. Different dissociation pathways are collectively induced and their interference contributes to the kinetic-energy release spectra. Chirping is able to efficiently manipulate the interferences of different dissociation pathways. We demonstrate a linear relationship between chirp and CEP dependent dissociation as well as directional electron localization.

DOI: 10.1103/PhysRevA.100.063409

The advent and steady evolution of ultrashort intense laser sources and momentum imaging techniques have placed the research in the fields of ultrafast strong-field-matter interaction in general and photodissociation and ionization processes in particular into attention [1–14]. The simplest molecules available, i.e., the molecular hydrogen and its ionic companion, have been used as standard models to examine the underlying complex dynamics arising when they are illuminated by strong and short light fields. Particularly interesting phenomena, such as bond softening and above-threshold dissociation, have been experimentally demonstrated successfully in these elementary molecular systems [4,10,11,14–16]. Amongst the knobs available to manipulate and control these phenomena, laser peak intensity, carrier envelope phase, and pulse duration have predominantly been used [7,17–19]. It is possible, however, to manipulate the temporal and spectral shape of the driving laser sources [20], thanks to the spectrally broad bandwidth of femtosecond pulses. The linear chirp, the linearly instantaneous central frequency change, in the form $\omega(t) - \omega_0 \propto \eta t/\tau^2$, across the bandwidth of the pulse, configures the simplest example of such control, where ω_0 is the central frequency, τ is the pulse length, and η is a unitless parameter to define the linear chirp. Pulses in which the lower frequencies come behind (ahead) are referred to as negatively (positively) chirped. More involved manipulation schemes can be used though, including nonlinear chirped pulses [21] and multicolor laser sources [22]. Applications of chirped pulse control include controlling atomic collisions [23], resonant high-order harmonic generation [24], above threshold ionization [25], single attosecond pulse generation [26], controlling the population transfer in rovibrational states [27,28], and imaging coupled electron-nuclear dynamics [29]. The theoretical and experimental complexity of them, however, make linear chirped pulses still one of the most suitable drivers for gaining systematic knowledge. In particular, the manipulation of bond hardening and selective bond dissociation and dissociative ionization using linearly chirped pulses were demonstrated [8,29,30]. We should note, however, that none of these studies have specifically reported relevant impacts on photodissociation due to chirp, such as that of the carrier-envelope offset phase.

Chirping the laser pulse not only introduces polychromy with certain gradients, but also directly reduces the intensity by $I_0/(1+\eta^2)$ and increases the temporal pulse bandwidth $(1+\eta^2)\tau_0$ due to group delay dispersion (GDD), where I_0 and τ_0 are the intensity and duration of the transform-limited (TL) pulse, respectively. Reduction in intensity or ending up with a longer pulse is certainly undesirable for ultrashort laser pulse generation and for efficient molecular dissociation due to the fact that pulse elongation via chirp makes the dissociation rate suppressed [31] as well as disrupts CEP control, which are both crucial for directional control of molecular reactions. To overcome these issues in chirping, one can consider a phenomenological waveform synthesis, which we call temporal-bandwidth-maintaining chirping scheme, where the intensity and the duration are kept fixed for varying chirps. This would allow one to generate such extremely short and chirped pulses. We anticipate that this concept allows a robust investigation of coherent control over the dissociation dynamics of molecules.

We consider the chemical reaction $H_2 + \gamma \rightarrow H_2^+ + e^- + \gamma \rightarrow H + p + e^-$, where γ is the chirped field. Here, we consider the situation that H_2^+ is dynamically populated directly from the ionization of H_2, at some time t_i, by the chirped laser field. In this study, MO-ADK [32] rates are used to determine the ionization rates and ionization times. Time-dependent Schrödinger equation (TDSE)

$$i\frac{\partial\Psi(\mathbf{r},R,t>t_i)}{\partial t} = H(\mathbf{r},R,t>t_i)\Psi(\mathbf{r},R,t>t_i) \quad (1)$$

is then solved for H_2^+ in chirped laser fields. For a preliminary understanding of the chirp effect on CEP-controlled dissociation, we first investigated the two-level model for the dissociation of H_2^+ with chirped laser pulses, based on the ansatz that the wave function is expanded in terms of attractive ground $1s\sigma_g$ (gerade) and repulsive first excited

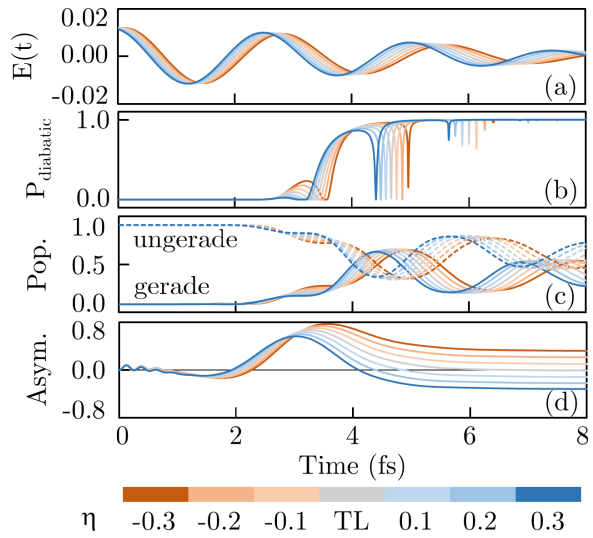

FIG. 1. Chirp effect on the dissociation of H_2^+ in a two-level system. All gray (blue) [brown] lines for transform limited (positively perturbed) [negatively perturbed] pulses. (a) Temporal variation of the chirped pulse. $\phi_0 = 0$. (b) Landau-Zener probability from adiabatic to diabatic process. (c) Left (solid) and right (dashed) populations over the ungerade and gerade states. (d) Asymmetry change by chirp. It changes sign with the change in the sign of chirp.

$2p\sigma_u$ (ungerade) states as $\Psi(\mathbf{r}, R, t) \simeq \psi_g(R, t)\phi_g(\mathbf{r}; R) + \psi_u(R, t)\phi_u(\mathbf{r}; R)$ (see, e.g., Ref. [33]),

$$\begin{bmatrix} i\dot{\psi}_g(R,t) \\ i\dot{\psi}_u(R,t) \end{bmatrix} = \begin{bmatrix} -\nabla^2/2\mu_p + V_g(R) & -\mu(R)F(t) \\ -\mu(R)F(t) & -\nabla^2/2\mu_p + V_u(R) \end{bmatrix} \times \begin{bmatrix} \psi_g(R,t) \\ \psi_u(R,t) \end{bmatrix}, \quad (2)$$

in which we consider a perturbative chirping, i.e., $|d\omega(t)/dt| \ll 1$. Here, R is the nuclear separation, μ_p is the reduced mass of the nuclei, $V_{g/u}(R)$ are the diabatic potentials, $\psi_{g/u}(R, t)$ are the nuclear wave functions of the gerade or ungerade states, and $\mu(R)$ is the transition dipole of H_2^+. For a clear understanding, we take the initial wave packet to be at the electronically excited ungerade state since, otherwise, a large residue of the initial state would remain in the ground state [33,34]. For the two-level model, we assume that H_2^+ was born at $t_i = 0$. To determine the interstate transitions and dynamical origin of such transitions (i.e., adiabatic, diabatic, or mixed dynamics), we calculate the avoided-crossing passage probability by the Landau-Zener formula as $P_{\text{diabatic}}(R, t) = \exp\{-\pi V_{ug}(R)^2/[4\omega_0\mu(R)F(t)]\}$, where $V_{ug}(R) = V_u(R) - V_g(R)$ is the coupling between the states and $F(t)$ is the time-dependent laser field, in the form $F(t) = E_0 \exp[-4\ln(2)\frac{t^2}{\tau^2}]\cos(\omega_0 t + \phi_0 + \frac{4\ln(2)\eta}{\tau^2}t^2)$ in our study. ϕ_0 is the CEP of the TL pulse and τ is the duration (at FWHM) of the pulse. Here, $V_{ug}^2 \gg \omega_0\mu F$ and $V_{ug}^2 \ll \omega_0\mu F$ conditions correspond to a completely adiabatic and completely diabatic transition dynamics, respectively. We define an asymmetry parameter, $A = (P_R - P_L)/(P_R + P_L)$, to quantify the directional electron localization, where $P_{R/L}$ corresponds to localization at the right or left nucleus. Figure 1 shows that the adiabatic part, where the wave packet stays in the ungerade state, finishes at ∼2.5 fs and the diabatic part starts at ∼6.2 fs for the TL pulse, where the wave packet occasionally jumps between the states, i.e., at the zero crossings of the field [see Fig. 1(c)]. For positive (negative) chirp values, these happen earlier (later). For positive chirp, higher frequencies appear later in the falling edge, resulting in a more rapid change per cycle [see Fig. 1(a)]. Electronic transitions happen earlier, maximum transition probability per-cycle is reduced, and localization is established in the left nucleus ($A < 0$), after which the electron population freezes out [see Fig. 1(d)]. For negative chirp, the falling edge is at lower frequencies; the electronic transitions happen later and maximum transitions per cycle are increased, resulting in an increased asymmetry in the mixed (adiabatic + diabatic) dynamics part (i.e., within 2–6 fs). The electron localization is therefore established in the right nucleus ($A > 0$). Regardless of the sign of chirp, absolute asymmetry is enhanced relative to that of the TL pulse and a linear variation of asymmetry with chirp in the form of $A \propto -\eta$ is found [see Fig. 1(d)].

For a complete theoretical picture on the chirp effect in ultrashort dissociation of H_2^+, we solved TDSE and obtain the kinetic-energy release (KER) of dissociation by chirped pulses to calculate CEP dependence of dissociation and asymmetry. We employed the numerical solution of the TDSE, defined as

$$i\frac{\partial}{\partial t}\Psi(\mathbf{r}, R, t) = [T_e + T_n + V_e(r, R) + V_n(R) + zF(t)]\Psi(\mathbf{r}, R, t), \quad (3)$$

where T_e and T_n are the kinetic energy of the electron and nuclei, $V_e(r, R)$ and $V_n(R)$ are the interaction terms for electron-nuclei and nucleus-nucleus, respectively, and the last term is the molecule-field interaction potential for a linearly polarized pulse. The procedure for the solution of Eq. (3) is provided in Ref. [35]. We choose a two-cycles field at FWHM with wavelength 800 nm and with an intensity of 150 T W/cm^2. We use the same form of the chirped laser field, mentioned previously. We assume that H_2^+ is produced by on-the-fly ionization of the neutral hydrogen molecule at $t = t_i$, with Franck-Condon (FC) distributed vibrational levels on $1s\sigma_g$ potential curve and we examined different chirp values between $\eta = -0.7$ and $\eta = 0.7$. MO-ADK rates are used to determine the ionization rates and ionization times [32], namely,

$$w_{\text{ion}}(t) = Q\sqrt{\frac{3F}{\pi\kappa^3}}\frac{1}{\kappa^{(2Z_c/\kappa)-1}}\left(\frac{2\kappa^3}{F}\right)^{2Z_c/\kappa-1} e^{-2\kappa^3/3F}, \quad (4)$$

where $Q = 3.5$, $\kappa = \sqrt{2I_p}$, Z_c is the effective charge, and $F = F(t; \phi)$ is the electric field. Figure 2 shows the time-dependent ionization rates, $w_{\text{ion}}(t)$, of H_2, forming H_2^+, subjected to an ultrashort chirped laser field. In order to demonstrate the impact of chirping the laser field on the time-dependent ionization, we first calculate the ionization rates of H_2 for zero CEP, as shown in Fig. 2(a). In this case, the ionization appears to have three peaks separated by a half-cycle: one main peak at $t = 0$ and two satellite peaks at the rising and falling edge of the laser field. These peaks are caused by the maxima of the laser field around $t = 0$. Beyond $|t| >$ 2 fs the ionization rates are considerably small. Chirping the laser field causes a linear increase (decrease) and linear left

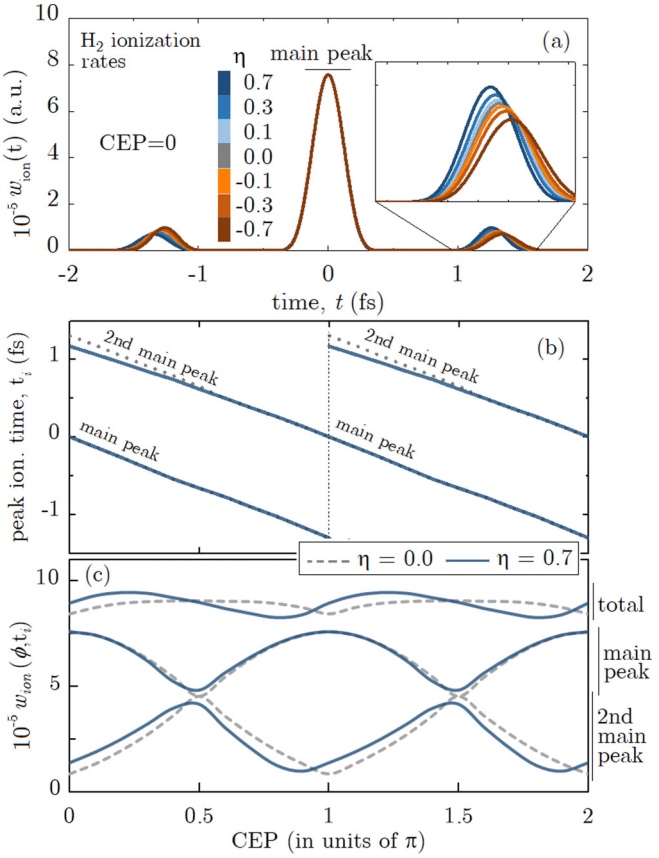

FIG. 2. MO-ADK calculated time-dependent ionization rates of H_2, forming H_2^+, by a chirped laser field. (a) Temporal variation of the ionization rates, $w_{\rm ion}(t)$, in -2 fs $< t < 2$ fs for different chirp values. Inset is a zoom to the temporal range 1 fs $< t <$ 1.6 fs. (b) Ionization time t_i of the main and second main peak as a function of CEP for TL and positively chirped pulse. (c) Ionization rates of the main and second main peak at $t = t_i$ as a function of CEP. "Total" corresponds to the sum of the ionization rates of these two peaks. An 800 nm Gaussian pulse with two cycles at FWHM and $I =$ 150 TW/cm^2 is used.

(right) shift in ionization rates of H_2 for positive (negative) chirps in the right satellite peak compared to those from the TL pulse. However, $w_{\rm ion}(t)$ decrease (increase) with positive (negative) chirp for the left satellite peak but they are still left (right) shifted. Figure 2(b) shows the CEP dependence of the ionization time, t_i, of the main and the second main peak for TL and a positively chirped pulse, $\eta = 0.7$. We observe that t_i changes linearly with CEP and chirping the field does not effect the ionization time of the main peak but causes a slight down shift in the second main peak at $t > 0$ for $\phi_0 = 0 - \pi/2$. As shown in Fig. 2(c), the instantaneous ionization rate at t_i, i.e., $w_{\rm ion}(t_i)$, of the main and second main peak oscillate with ϕ_0 with π periodicity. The oscillations of the main peak are almost unaffected by the chirp, except around $\phi = \pi/2$, but the second main peak significantly left shifted. The peaks unite at $\phi = \pi/2$ since these two peaks become identical (due to the time profile of the laser field at $\phi = \pi/2$) and are separated by a half-cycle at this phase.

Next, we calculate the chirped-field-induced dissociation of H_2^+ for $t > t_i$, i.e., following the ionization of H_2. In order to calculate the kinetic-energy release (KER) spectra of the field-induced dissociation, i.e., $H_2^+ + \gamma \rightarrow p^+ + H$, we employ the so-called "virtual-detector" method [36]. In this approach, we first define $k(R_d, t) = mj(R_d, t)/\rho(R_d, t)$ as the time-dependent wave-packet momentum, calculated at point $R = R_d$, where we position the virtual detector at $R_d = 10$ a.u., $j(R_d, t)$ is the flux-density operator, $j(R_d, t) = \frac{1}{m}\mathrm{Re}[\langle\Psi(t)|\widehat{p}|\Psi(t)\rangle]|_{R=R_d}$, and $\rho(R_d, t)$ is the probability of finding the particle at $R = R_d$. m is the mass of the particle. In order to derive the KER distribution $P(E)$ of H_2^+ born at $t > t_i$ we use

$$P(E)|_{E=k'^2/2\mu} \propto \int dt\; j(R_d, t)\delta(k' - k(R_d, t)), \qquad (5)$$

where, for the numerical evolution, a binning-histogramming procedure is necessary.

As previously described, the dissociation process of H_2^+ is activated when the neutral H_2 is dynamically ionized with a certain time-dependent probability. Therefore, one can speak of a coherent accumulation of the dissociation process for H_2^+, since dissociative ionization is coherent. In other words, when H_2 is ionized with a certain probability at a certain time, there is still population in H_2, while there is already dynamics going on in H_2^+ under the influence of the laser field. When the next ionization arrives, nuclear population is again transferred to H_2^+, which may couple with the preceding event where the weight of the latter can be determined by the relative ionization probability. A complete numerical solution of TDSE for neutral H_2 needs to be considered to take into account all effects. Instead, we employ a simplified model where we assume that the wave packet of H_2^+ propagates and at each time step a fresh wave packet from H_2 is transferred when ionized. The phase difference between successive ionization events determines the extent to which H_2^+ cations interfere [37]. Therefore, in one extreme case H_2 ionizes at different times and the phase difference yields that the launched wave packets do not interfere. In this case, since the asymmetry is caused by coherent superposition within individual molecules, the asymmetry (as well as dissociation) results add up incoherently. The total KER of dissociation of H_2^+, formed by the ionization of H_2 at any t_i, in a chirped laser field can then be determined from

$$P_{\rm tot,incoh}(E) \propto \int w_{\rm ion}(t_i)P(E, t_i)dt_i, \qquad (6)$$

where $w_{\rm ion}(t_i)$ is the ionization rate of H_2 at instant t_i and $P(E, t_i)$ is the dissociation probability of H_2^+ born at t_i. Here, we employed Eq. (5) for the prediction of $P(E, t_i)$ for $t > t_i$. The integration in Eq. (6) can be approximated in the form $\int dt \simeq \Sigma_n \delta(t - nT(t)/2)$, where $T(t) = 2\pi/\omega(t)$ is the time-dependent period of the chirped field, since ionization is effectively high at the maxima of the pulse [see, e.g., Fig. 2(a)]. Therefore, in our calculations we take $P_{\rm tot,incoh}(E) \propto \Sigma_n w_{\rm ion}(t_i)P(E, t_i)\delta(t_i - nT(t)/2)$ for the total dissociation. In the opposite extreme, we consider a maximal coherence between the launched wave packets. Hence we calculate an approximate H_2^+ wave function

$$\Psi(\mathbf{r}, R, t) = \Psi_1(\mathbf{r}, R, t; t_1) + \int w_{\rm ion,rel}(t_i)H(t - t_i)\Psi_i(\mathbf{r}, R, t; t_i)dt_i \qquad (7)$$

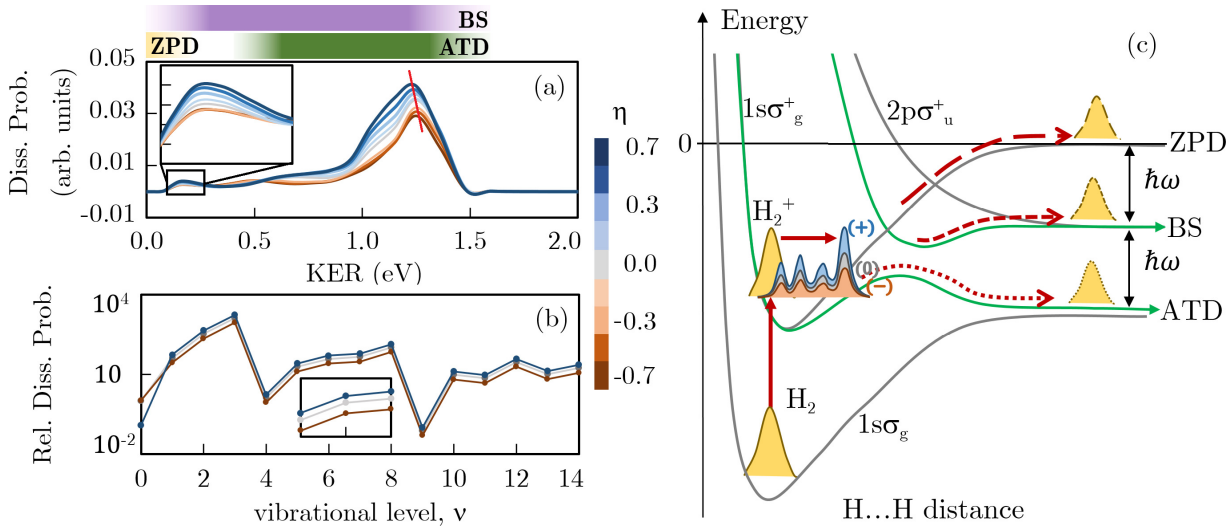

FIG. 3. (a) Variation of CEP-integrated KER spectra of dissociation by chirp. Inset: zoom in to the 0.1–0.3 eV interval. (b) Contributions to the dissociation from different vibrational levels. Inset: zoom in to the fifth–seventh vibrational states. (c) Energy curves of diabatic (gray) gerade and ungerade states (green) and possible BS and ATD dissociation channels. Diagram also illustrates how positive (+), transform-limited (0), and negative (−) chirp influence vibrational population transfer to the same vibrational state, based on (b). Laser parameters are the same as in Fig. 2.

as the coherent accumulation, where $\Psi_i(\mathbf{r}, R, t; t_i)$ is the wave function of H_2^+ launched at t_i, $H(t - t_i)$ is the Heaviside step function, and $w_{ion,rel}(t_i) = w_{\rm ion}(t_i)/w_{\rm ion}(t_1)$ is the relative ionization rate of H_2, found from Eq. (4). However, as we approximate the integration in Eq. (6) with a summation, it is also convenient to approximate the integral in Eq. (7). In this case, Eq. (7) can be written as

$$\Psi(\mathbf{r}, R, t) = \Psi_1(\mathbf{r}, R, t; t_1) + \sum_n w_{\rm ion,rel}(t_n) H(t - t_n) \Psi_n(\mathbf{r}, R, t; t_n), \quad (8)$$

where $t_n = nT(t)/2$. Thus the energy-dependent dissociation probability for a maximal coherent case is calculated from

$$P_{\rm tot,coh}(E) \propto w_{\rm ion}(t_1) P(E). \quad (9)$$

We base the first part of our calculations and results on the incoherent accumulations of the wave packet by eliminating the interference of the wave packets in order to elaborate the impact of individual cations. In the next section we calculate the impact of coherent accumulation of the wave packets. In all cases, we assumed that launched wave packets are initially in the FC distributed vibrational levels on the $1s\sigma_g$ states.

I. INCOHERENT ACCUMULATION CALCULATIONS

There is a linear increase in dissociation probability by chirp which can be seen in Fig. 3(a). The increase is even more dramatic within the KER range of 1.0–1.3 eV. The maximum of the distribution appears to be left shifted, consistent with the recent experiments for longer pulses [30,38]. To understand such variations, we have calculated the level-resolved contributions to dissociation. Different channels, launched by photon transitions between electronic states and at different vibrational states, contribute to dissociation. Identification of these channels through KER is necessary to determine the physical mechanism responsible for dissociation [15]. Typically, in the low (i.e., 0–3 eV) KER region three major electronic transitions between the ground ($1s\sigma_g$) and the first excited state ($2p\sigma_u$) lead to dissociation: (i) zero-photon dissociation (ZPD), $1s\sigma_g + \omega - \omega \rightarrow 1s\sigma_g$ transition, i.e., absorption of net zero photons, (ii) bond softening (BS), $1s\sigma_g + \omega \rightarrow 2p\sigma_u$, i.e., absorption of net one photon, and (iii) above-threshold dissociation (ATD), $1s\sigma_g + 3\omega \rightarrow 2p\sigma_u \rightarrow 1s\sigma_g + \omega$, i.e., absorption of net two photons. Therefore, $E_{\rm KER} = n\omega - |E_\nu|$ yields the energy of the dissociating wave packet from different channels, where E_ν is the vibrational energy and n is the number of net absorbed photons. Here, to eliminate the time dependence of the laser frequency due to chirp, we considered a time-averaged frequency as $\langle\omega\rangle = \omega_0 + \eta/\tau$ for the analysis of the results. First, $\langle E_{\rm KER}\rangle = n[\omega_0 + \eta/\tau] - |E_\nu|$, in fact, enounce that the kinetic energies of the dissociating wave packet are independent of chirp, since lower (higher) vibrational levels would in turn contribute to KER if positive (negative) chirp is used. To demonstrate this, for a TL pulse ($\eta/\tau = 0$) with $\lambda =$ 800 nm (and $\omega_0 = 1.55$ eV), the KER of H_2^+ dissociation through the BS ($n = 1$) channel is launched from the $\nu = 5$ and higher levels. But when $\eta/\tau = 0.1$ eV and $\omega_0 = 1.55$ eV, this threshold becomes $\nu = 4$. Therefore, the variation of KER spectra with chirp is caused by the variations in vibrational excitations. To support this, we calculated the chirp dependence of the dissociating vibrational population rates based on the projections of the dissociating wave packet to each vibrational state, ν, for positive, TL, and negative chirp values. As shown in Fig. 3(b), and with the help of the diagram in Fig. 3(c), we find that the vibrational levels are coherently depopulated with positive (negative) chirp relative to the TL pulse. Its effect is more pronounced within the KER range 1.0–1.3 eV, since both $\nu > 9$ rendering the BS channel and the first few ν rendering the ATD channel (and which are at high populations) collectively contribute to this KER range [see Figs. 3(a)–3(c)]. To conclude, the variation of KER in the dissociation

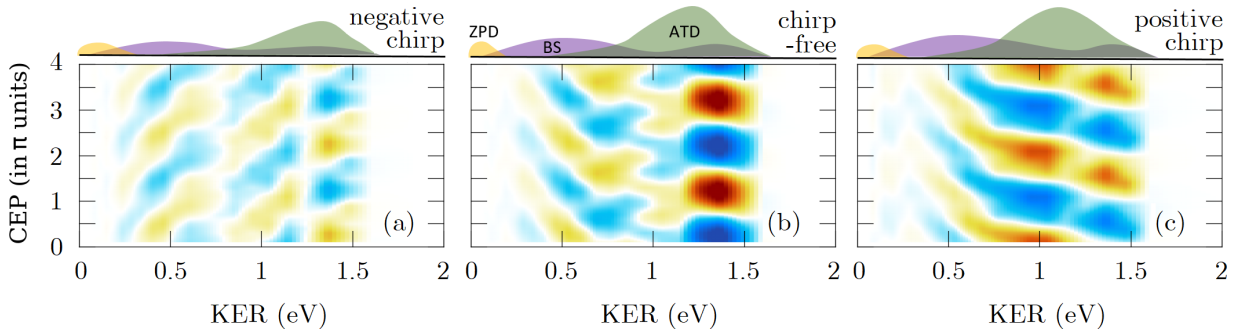

FIG. 4. Asymmetry maps for (a) negative chirp ($\eta = -0.7$), (b) transform limited case ($\eta = 0$), and (c) positive chirp ($\eta = 0.7$) cases. Top panel: contributions of different dissociation channels to KER determined from Fig. 3.

probability is directly related to the variations in vibrational population transfer by chirp and the dissociation channel.

We next calculate the CEP dependence of dissociation probability and electron-localization asymmetry in ultrashort chirped laser pulses. The energy-resolved electron-localization asymmetry, $A(E, \phi)$, is computed from $A = (P_R - P_L)/(P_R + P_L)$ with the help of Eq. (3), where $P_{R/L}(E, \phi)$ correspond to dissociation through the right or left. Chirped CEP is indeed time dependent having the analytical form $\phi(t, \eta) = \phi_0 + \eta t^2/\tau^2$, where $\eta t^2/\tau^2$ can be considered as the instantaneous phase variation in CEP, i.e., "phase of the phase" [39]. To comprehend how chirp affects the CEP dependency of dissociation probability and asymmetry, we time averaged the chirped CEP as a first-order approximation and found that $\langle\phi(t, \eta)\rangle = \phi_0 + 4\eta/3$. This indicates that the phase of the phase typically varies linearly by $4\eta/3$ with chirp.

We calculate the KER-CEP maps of the dissociation and asymmetry for various chirp values and present CEP variation of asymmetry results with KER integration over different energy ranges. First, Fig. 4 shows the impact of zero, positive, and negative chirp values on asymmetry. One can see a strong chirp modulation in the CEP-dependent asymmetry. Asymmetry maps for the negative chirp consist of uphill diagonal weak stripes modulating with CEP and increasing KER as shown in Fig. 4(a). However, these stripes appear to be downhill for the positive chirp with enhanced asymmetry (*vide infra*).

Figure 5 shows the CEP variations in the chirp dependent KER-integrated asymmetry for different KER regions. For the high-energy region the amplitude of asymmetry of dissociation linearly decreases and CEP dependence right shifts for both positive and negative chirps. For the midenergy region the amplitude linearly enhances and the CEP dependence right shifts from negative up to positive chirp. Finally, in contrast to the midenergy case, for the low-energy region the amplitude of asymmetry reduces and right shifts. Specifically, a linear fitting of the η variation in the CEP positions of the maxima for the 1.3–1.5 eV region, 0.8–1.0 eV region, and 0.1–0.3 eV region (see Fig. 5) gave a slope of 1.21 ± 0.09, 1.40 ± 0.12, and 1.92 ± 0.45, respectively, which are consistent with $4/3$ ($\simeq$1.33) in the first-order approximation for CEP, i.e., $\langle\phi(t, \eta)\rangle = \phi_0 + 4\eta/3$. Based on these considerations, one can, in general, approximate the CEP variation of asymmetry for a certain chirp in the form of $A(\phi, \eta) \simeq A_0(\eta)\cos(\phi)$, where $\phi = \phi(\eta)$ (see Fig. 5).

Even though there is a linear relationship between the chirp and the CEP dependence of asymmetry, it is clear that the mechanism behind the right-left shifts and the variation in the amplitudes for different chirp values and for different KER regions is much more complicated as presented in Fig. 4. But, apparently, our analysis of the dissociation probability and its relation to the dissociation pathways show that they are playing the central role here. Besides, in general, interferences between states with different parity, e.g., between gerade and ungerade states in the case of H_2^+, are needed to achieve asymmetry in electron localization [40]. Such superpositions can be reached by interferences of different dissociation paths such as ZPD and BS or BS and ATD. However, as in our case, this asymmetry can also be established in a single dissociation path with varying photon-transition energies in chirped pulses. The ZPD-BS interference and BS-ATD interference produce asymmetry in the low and the remaining (mid and high) regions, respectively. For the low KER (0.1–0.3 eV), $\nu \simeq$ 5–7 levels contribute to BS and very high ν values contribute to ZPD in ultrashort pulses, but their probabilities are low [see Fig. 3(b)]. The decreasing amplitude in the asymmetry from

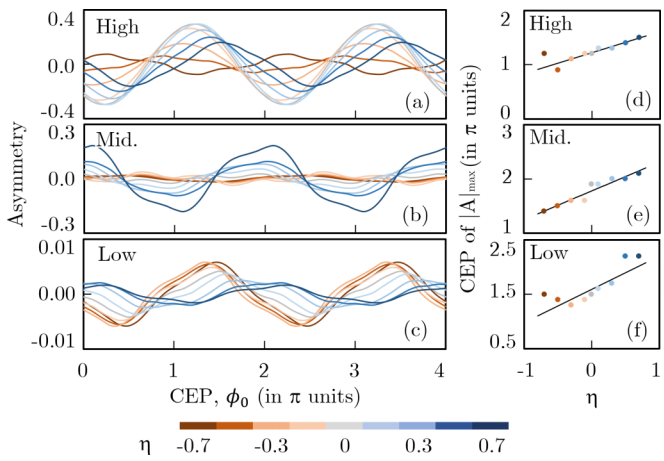

FIG. 5. KER-integrated asymmetry for incoherent calculations for (a) high- (1.3–1.5 eV), (b) middle- (0.8–1.0 eV), and (c) low- (0.1–0.3 eV) energy regions. Fits for $|A_{max}|$ for (d) high-, (e) middle-, and (f) low-energy regions. CEP variation shifts to the left or right depending on the energy region linearly with chirp, consistent with the first-order approximation of the impact of chirped CEP on asymmetry. Laser parameters are the same as in Fig. 2.

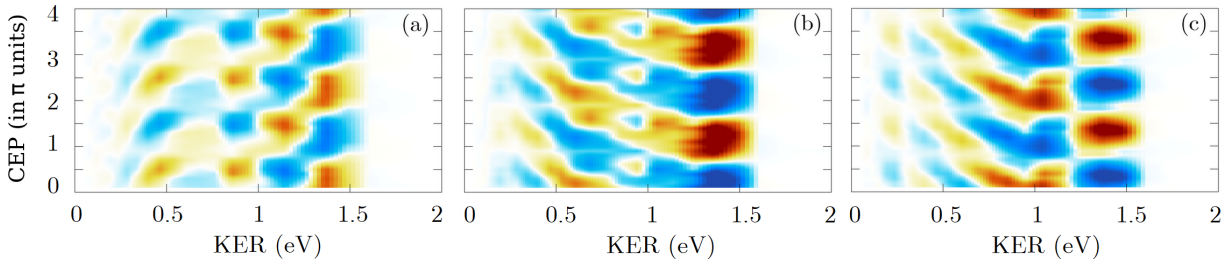

FIG. 6. Asymmetry maps from the coherent accumulation of the wave packets for (a) negative chirp ($\eta = -0.7$), (b) transform limited case ($\eta = 0$), and (c) positive chirp ($\eta = 0.7$) cases.

negative to positive η observed for the low KER in Fig. 4 is due to the systematic increase in the dissociation from BS relative to ZPD in this KER region. In other words, increasing dissociation from BS relative to ZPD results in an overall decrease in the overlap of ZPD-BS KER regions. This is also evident from the systematic increase in the dissociation in the low KER region shown by the inset of Fig. 3(a). For the high KER range (1.3–1.5 eV) the asymmetry of the negative chirp [in Fig. 4(a)] decreases relative to the TL pulse, which can be attributed to the decreasing dissociation rate for both BS and ATD in this region. The decrease in the asymmetry for the positive chirp—even though dissociation rate increases—is due to the shift of ATD to lower KER region, resulting in reducing BS-ATD overlap. These are also in compliance with increasing asymmetry around mid KER region 0.8–1.0 eV for positive chirp as well as weak asymmetry for the negative chirp in the same region relative to the TL pulse, as shown in Fig. 4.

II. COHERENT ACCUMULATION CALCULATIONS

In this part, with the aid of Eqs. (8) and (9), we calculate the dissociation and asymmetry of H_2^+ in chirped pulses by considering a coherent accumulation of the wave packets, i.e., assuming that the individually launched H_2^+ wave packets dynamically interfere within the laser pulse. We calculated the dissociation using Eq. (5) and the asymmetry via $A = (P_R - P_L)/(P_R + P_L)$. The KER-CEP maps in Fig. 6 show that the overall appearances for different chirp values are similar to those we obtained for the incoherent case shown in Fig. 4, which suggests that the energetic contributions of the dissociating pathways responsible for the KER-CEP maps in the coherent accumulations are nearly the same as for the incoherent case. However, looking at the fine structures and comparing them with those in Fig. 4, we observe that there are slight differences in asymmetry between incoherent and coherent cases around half integer π values of CEP but the difference is less for the integer π values. This stems from the fact that for the latter a sole strong peak at $t = 0$ predominantly contributes (see Fig. 2) to the dissociative ionization process.

There is still CEP-dependent oscillations in asymmetry for different KER regions and we observed a linear relationship between η and CEP for the coherent case, as shown in Fig. 7. Fit results for coherent calculations give slopes 2.77 ± 0.32, 1.94 ± 0.29, and 3.38 ± 0.70 for high (1.3–1.5 eV), middle (0.8–1.0 eV), and low (0.1–0.3 eV) KER regions, respectively. The results are systematically higher than those of the incoherent accumulation and also the first-order approximation for the phase of the phase (i.e., $\langle\phi(t,\eta)\rangle = \phi_0 + 4\eta/3$) appears to underestimate the slopes (i.e., 4/3) for the coherent case. Specifically, the correlation between η and asymmetry seems to be relatively weak in the low-energy range for both incoherent and coherent accumulations due to very fine-scale oscillations and complexity in the asymmetry with KER in this range.

In conclusion, we have investigated the chirp effect on CEP-controlled dissociation and asymmetry and found that exploiting the chirp modulates electron localization during dissociation. Dissociation is enhanced by chirp and CEP dependence of both the dissociation and the asymmetry shift with the chirp parameter. We find that ZPD, BS, and ATD pathways are selectively induced depending on the sign and value of chirp and their interferences alternatively contribute to the KER spectra. We explored the dissociation dynamics in the context of incoherent and coherent accumulations of the individual H_2^+ wave packets launched at different phases, arising from the strength of the wave-packet interferences. We found a linear relationship between the chirp and asymmetry in electron localization for both cases. We anticipate that our results for the chirped pulses provide an alternative perspective in the subcycle control of electron dynamics in molecular reactions.

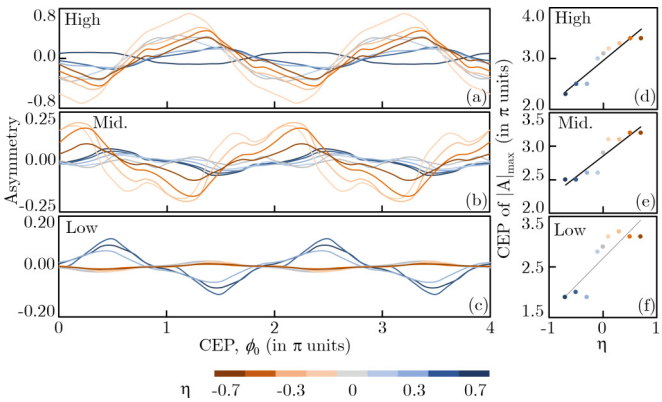

FIG. 7. KER-integrated asymmetry for coherent calculation for (a) high-, (b) middle-, and (c) low-energy regions. Fits for $|A_{max}|$ for (d) high-, (e) middle-, and (f) low-energy regions. CEP variation shifts to the left or right depending on the energy region linearly with chirp. Here first-order approximation underestimates the impact of chirp on asymmetry. Laser parameters are the same as in Fig. 2.

ACKNOWLEDGMENTS

S.A.B. and I.Y. are grateful for the support by the Research Fund of Marmara University, Project No. FEN-C-DRP-230119-0005. S.A.B. is partially supported by the Turkish Funding Agency, TUBITAK, by the 2211 Graduate Bursary Program. P.R. and M.F.K. are grateful for support by the German Research Foundation via Grant No. KL1439/11-1 and the center of excellence "Munich Centre of Advanced Photonics." This work was supported by the project Advanced research using high intensity laser produced photons and particles (No. CZ.02.1.01/0.0/0.0/16_019/0000789) from European Regional Development Fund (ADONIS). Computing resources for simulations used in this work were provided by the National Center for High Performance Computing of Turkey (UHeM) under Grant No. 5005902018. Data analysis are performed at the Simulations and Modelling Research Lab (Simulab), Physics Department of MU.

[1] A. M. Sayler, P. Q. Wang, K. D. Carnes, B. D. Esry, and I. Ben-Itzhak, Phys. Rev. A **75**, 063420 (2007).

[2] H. G. Breunig, A. Lauer, and K.-M. Weitzel, J. Phys. Chem. A **110**, 6395 (2006).

[3] J. McKenna, A. M. Sayler, B. Gaire, N. G. Johnson, E. Parke, K. D. Carnes, B. D. Esry, and I. Ben-Itzhak, Phys. Rev. A **77**, 063422 (2008).

[4] K. Sändig, H. Figger, and T. W. Hänsch, Phys. Rev. Lett. **85**, 4876 (2000).

[5] I. D. Williams, P. McKenna, B. Srigengan, I. M. G. Johnston, W. A. Bryan, J. H. Sanderson, A. El-Zein, T. R. J. Goodworth, W. R. Newell, P. F. Taday, and A. J. Langley, J. Phys. B **33**, 2743 (2000).

[6] I. Ben-Itzhak, P. Q. Wang, J. F. Xia, A. M. Sayler, M. A. Smith, K. D. Carnes, and B. D. Esry, Phys. Rev. Lett. **95**, 073002 (2005).

[7] M. F. Kling, C. Siedschlag, A. J. Verhoef, J. I. Khan, M. Schultze, T. Uphues, Y. Ni, M. Uiberacker, M. Drescher, F. Krausz, and M. J. J. Vrakking, Science **312**, 246 (2006).

[8] L. J. Frasinski, J. H. Posthumus, J. Plumridge, K. Codling, P. F. Taday, and A. J. Langley, Phys. Rev. Lett. **83**, 3625 (1999).

[9] A. Assion, T. Baumert, U. Weichmann, and G. Gerber, Phys. Rev. Lett. **86**, 5695 (2001).

[10] J. McKenna, M. Suresh, D. S. Murphy, W. A. Bryan, L.-Y. Peng, S. L. Stebbings, E. M. L. English, J. Wood, B. Srigengan, I. C. E. Turcu, J. L. Collier, J. F. McCann, W. R. Newell, and I. D. Williams, J. Phys. B **40**, 2607 (2007).

[11] J. H. Posthumus, J. Plumridge, L. J. Frasinski, K. Codling, E. J. Divall, A. J. Langley, and P. F. Taday, J. Phys. B **33**, L563 (2000).

[12] D. Pavičić, T. W. Hänsch, and H. Figger, Phys. Rev. A **72**, 053413 (2005).

[13] B. Feuerstein, T. Ergler, A. Rudenko, K. Zrost, C. D. Schröter, R. Moshammer, J. Ullrich, T. Niederhausen, and U. Thumm, Phys. Rev. Lett. **99**, 153002 (2007).

[14] P. Q. Wang, A. M. Sayler, K. D. Carnes, J. F. Xia, M. A. Smith, B. D. Esry, and I. Ben-Itzhak, Phys. Rev. A **74**, 043411 (2006).

[15] J. H. Posthumus, Rep. Prog. Phys. **67**, 623 (2004).

[16] J. McKenna, A. M. Sayler, F. Anis, B. Gaire, N. G. Johnson, E. Parke, J. J. Hua, H. Mashiko, C. M. Nakamura, E. Moon, Z. Chang, K. D. Carnes, B. D. Esry, and I. Ben-Itzhak, Phys. Rev. Lett. **100**, 133001 (2008).

[17] A. S. Alnaser and I. V. Litvinyuk, J. Phys. B **50**, 032002 (2017).

[18] H. Li, X. Gong, K. Lin, R. de Vivie-Riedle, X. M. Tong, J. Wu, and M. F. Kling, J. Phys. B **50**, 172001 (2017).

[19] H. Ibrahim, C. Lefebvre, A. D. Bandrauk, A. Staudte, and F. Légaré, J. Phys. B **51**, 042002 (2018).

[20] A. M. Weiner, Rev. Sci. Instrum. **71**, 1929 (2000).

[21] Z. Chang, *Fundamentals of Attosecond Optics* (Taylor and Francis Group, LLC, London, UK, 2011).

[22] H. Fattahi, H. G. Barros, M. Gorjan, T. Nubbemeyer, B. Alsaif, C. Y. Teisset, M. Schultze, S. Prinz, M. Haefner, M. Ueffing, A. Alismail, L. Vámos, A. Schwarz, O. Pronin, J. Brons, X. T. Geng, G. Arisholm, M. Ciappina, V. S. Yakovlev, D.-E. Kim, A. M. Azzeer, N. Karpowicz, D. Sutter, Z. Major, T. Metzger, and F. Krausz, Optica **1**, 45 (2014).

[23] M. J. Wright, J. A. Pechkis, J. L. Carini, S. Kallush, R. Kosloff, and P. L. Gould, Phys. Rev. A **75**, 051401(R) (2007).

[24] Z. Abdelrahman, M. Khokhlova, D. Walke, T. Witting, A. Zair, V. Strelkov, J. Marangos, and J. Tisch, Opt. Express **26**, 15745 (2018).

[25] J. Xu, B. Zeng, and Y. Yu, Phys. Rev. A **82**, 053822 (2010).

[26] Y. Niu, Y. Xiang, Y. Qi, and S. Gong, Phys. Rev. A **80**, 063818 (2009).

[27] C. Sarkar, R. Bhattacharya, S. S. Bhattacharyya, and S. Saha, Phys. Rev. A **78**, 023406 (2008).

[28] J. Plenge, A. Wirsing, C. Raschpichler, M. Meyer, and E. Rühl, J. Chem. Phys. **130**, 244313 (2009).

[29] D. Jelovina, J. Feist, F. Martín, and A. Palacios, New J. Phys. **20**, 123004 (2018).

[30] A. Natan, U. Lev, V. S. Prabhudesai, B. D. Bruner, D. Strasser, D. Schwalm, I. Ben-Itzhak, O. Heber, D. Zajfman, and Y. Silberberg, Phys. Rev. A **86**, 043418 (2012).

[31] A. Csehi, G. J. Halász, L. S. Cederbaum, and A. Vibók, J. Chem. Phys. **144**, 074309 (2016).

[32] X. M. Tong, Z. X. Zhao, and C. D. Lin, Phys. Rev. A **66**, 033402 (2002).

[33] F. Kelkensberg, G. Sansone, M. Y. Ivanov, and M. Vrakking, Phys. Chem. Chem. Phys. **13**, 8647 (2011).

[34] S.-I. Chu and D. A. Telnov, Phys. Rep. **390**, 1 (2004).

[35] I. Yavuz, M. F. Ciappina, A. Chacón, Z. Altun, M. F. Kling, and M. Lewenstein, Phys. Rev. A **93**, 033404 (2016).

[36] B. Feuerstein and U. Thumm, Phys. Rev. A **67**, 043405 (2003).

[37] F. He and U. Thumm, Phys. Rev. A **81**, 053413 (2010).

[38] V. S. Prabhudesai, U. Lev, A. Natan, B. D. Bruner, A. Diner, O. Heber, D. Strasser, D. Schwalm, I. Ben-Itzhak, J. J. Hua, B. D. Esry, Y. Silberberg, and D. Zajfman, Phys. Rev. A **81**, 023401 (2010).

[39] S. Skruszewicz, J. Tiggesbäumker, K.-H. Meiwes-Broer, M. Arbeiter, T. Fennel, and D. Bauer, Phys. Rev. Lett. **115**, 043001 (2015).

[40] V. Roudnev and B. D. Esry, Phys. Rev. Lett. **99**, 220406 (2007).